Morphology and Microtopology of Cation-Exchange Polymers and the Origin of the Overlimiting Current

J. Balster,[†] M. H. Yildirim,[†] D. F. Stamatialis,*[,†] R. Ibanez,[‡] R. G. H. Lammertink,[†] V. Jordan,[§] and M. Wessling[†]

Membrane Technology Group, Faculty of Science and Technology, University of Twente, Postbus 217, 7500 AE Enschede, The Netherlands, Department of Engineering Chemistry and Inorganic Chemistry, University of Cantabria, Avenida Los Castros, s/n, 39005 Santander, Spain, and Department of Chemical Engineering, Fachhochschule Münster, University of Applied Sciences, Stegewaldstrasse 39, 48565 Steinfurt, Germany

Received: December 10, 2006

In electrodialysis desalination processes, the operating current density is limited by concentration polarization. In contrast to other membrane processes such as ultrafiltration, in electrodialysis, current transport above the limiting current is possible. In this work, the origin of the overlimiting current at cation-exchange polymers is investigated. We show that, under certain experimental conditions, electroconvection is the origin of the overlimiting conductance. The theory concerning electroconvection predicts a shortening of the plateau length of membranes with increased conductive or geometrical heterogeneity. We investigate the influence of these two parameters and show that the creation of line undulations on the membrane surface normal to the flow direction, having distances in the range of approximately 50−200% of the boundary-layer thickness, lead to an earlier onset of the overlimiting current. The plateau length of the undulated membranes is reduced by up to 60% compared to that of a flat membrane. These results verify the existence of electroconvection as a mechanism destabilizing the laminar boundary layer at the liquid−membrane interface and causing ionic transport above the limiting current density.

1. Introduction

The optimization of membrane-based separation processes is strongly influenced by concentration polarization. Concentration gradients evolve in the feed at the membrane surface, leading to an imbalance of membrane resistance and hydrodynamic boundary-layer resistance. The boundary-layer resistance approaches values equal to the membrane resistance or even higher. In membrane processes such as pervaporation, vapor permeation, and ultrafiltration, concentration polarization is observed by the fact that the transmembrane flux does not increase with increasing driving force (transmembrane pressure) and reaches a limiting flux (J_{lim}) (see Figure 1a).[1] In electrodialysis, the limiting flux is called the limiting current density (i_{lim}). The voltage drop across the membrane is a measure of the driving force.[2−4] In contrast to the above-mentioned membrane processes, in electrodialysis, current transport above the limiting current is possible. If the driving force is increased beyond a critical voltage drop, the overlimiting current sets in, and transport occurs again (see Figure 1b).

Concentration polarization in electrodialysis is caused by differences between the ion transport number in the electrolyte solution and that in the ion-exchange membrane. The difference in transport number leads to depletion of salt ions on the dilute side of the membrane while the concentration near the membrane on the concentrated side simultaneously increases.[2,5] A typical current−voltage curve ($i-v$) of an ion-exchange membrane can be divided into three regions (Figure 2). The low-current ohmic region (region 1), a linear part giving the ohmic resistance of the membrane, is followed by a plateau (region 2, the limiting current density), caused by ion depletion in the hydrodynamic boundary layer. Inflection of the $i-v$ curve at

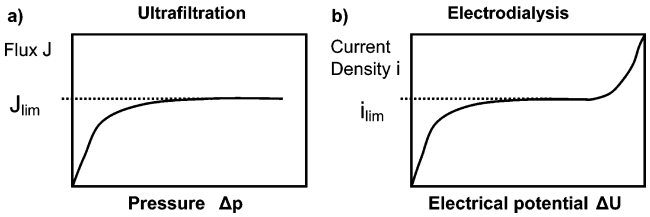

Figure 1. Comparison of the limiting flux in (a) ultrafiltration and (b) electrodialysis.

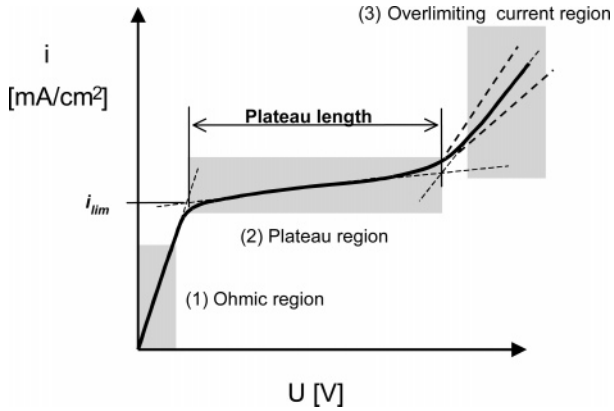

Figure 2. Schematic drawing of a typical $i-v$ curve of a monopolar ion-exchange membrane.

* Corresponding author. E-mail: d.stamatialis@utwente.nl. Tel.: +31-53-4894675. Fax: +31-53-4894611.
[†] University of Twente.
[‡] University of Cantabria.
[§] University of Applied Sciences.

10.1021/jp068474t CCC: $37.00
Published on Web 02/14/2007

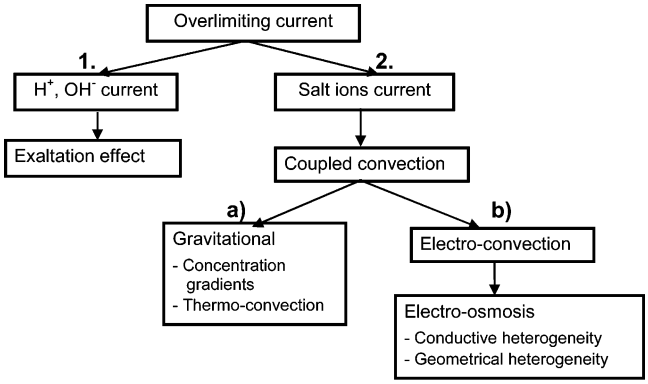

Figure 3. Possible secondary effects causing current growth above its limiting value, adapted from ref 9.

the plateau is followed by region 3, where the slope of the $i-v$ curve increases again and ion transport again sets in (overlimiting current region).[3] These values of the current density are normally averaged over time, because of fluctuations.

According to the theory of concentration polarization, currents larger than the limiting current density should not be expected. For a long time, region 3 was attributed to the generation of acid or base by the dissociation of water.[6] This hypothesis was based on experimental evidence of pH changes observed during desalination using anion-exchange membranes. Later, however, the absence of water dissociation at cation-exchange membranes diluted this argument.[7,8] The nature of the overlimiting flux has been disputed for some time, and different hypothesis based on two different transport mechanisms have been made (see Figure 3):[9] (1) The current is transported by protons and hydroxyl ions generated at the membrane−solution interface.[6,10] (2) The current is transported by salt ions through a secondary convective liquid flow called coupled convection.[9]

The mechanism of the overlimiting current depends on the treated electrolyte and its concentration,[11−13] the ion-exchange membrane,[1,6−8,13] and the construction of the electrodialysis cell.[9,13] The overlimiting current frequently has various origins, and it is difficult to distinguish the importance of the various origins. It is an experimental challenge to control the hydrodynamic and surface chemistry conditions to a degree that one can conclusively identify a single or multiple origins of the overlimiting current.

1.1. Current Transport by Protons and Hydroxyl Ions. The occurrence of the overlimiting current has been attributed to the dissociation of water, which was observed in terms of pH changes during desalination using anion-exchange membranes.[6] Protons and hydroxyl ions are generated and transported in a water dissociation layer formed between the ion-exchange membrane and the boundary layer. However, water dissociation efficient enough to cause overlimiting currents can be only achieved if the membrane contains ionic groups that catalyze the dissociation of water by protonation−deprotonation reactions.[14,15] Using detailed mass balances for cation- and anion-exchange membranes (containing ionic groups that do not catalyze water dissociation), Krol et al.[7,8] verified that the majority of the ion transport occurs through a different mechanism. In fact, they also found no loss of membrane permselectivity, which excludes the presence of additional charge carries. Using cation-exchange membranes, Choi et al.[11] and Tanaka[12] also showed that the contribution of water dissociation to the overlimiting current is very low. Only the presence on the surface of the cation-exchange membrane of metal ions such as Al^{3+}, Co^{2+}, Mg^{2+}, and Mn^{2+} that are able to form hydroxides can lead to strong water dissociation. The magnitude of water dissociation then also depends on the concentration of the metal ions.

From all the above points, it can be concluded that water dissociation is not the main cause of the overlimiting current: it contributes only when chemical groups that catalyze the water dissociation reaction are present.

1.2. Current Transport by Salt Ions. The fact that (especially) cation-exchange membranes do not lose permselectivity in the overlimiting current region suggests that the current is transported by counter ions (Figure 3).[7,8,11,15,16] Therefore, several scientists have suggested that the overlimiting behavior of ion-exchange membranes might be based on a convective mixing mechanism that develops spontaneously in the ion-depleted diffusion layer in an advanced state of concentration polarization. This convective mixing is called coupled convection.[17−19] Two mechanisms responsible for coupled convection have been considered: (1) gravitational convection caused by concentration or temperature gradients,[17,20] and (2) electroconvection caused by electric space charge localized near the solution−membrane interface.[21−30] The two mechanisms are described in more detail in the following sections.

Gravitational Convection. Gravitational convection (Figure 3) is caused by the Archimedes force, which appears in a membrane channel as a result of a nonuniform distribution of the electrolyte concentration (concentration gradient) and/or a nonuniform distribution of the electrolyte solution temperature (thermoconvection).[17,20] According to Zabolostsky et al.,[20] gravitational convection can play an important role only in membrane systems with sufficiently large intermembrane distances and electrolyte solution concentrations and low solution flow velocities. They calculated that, in wide membrane channels (distance between membranes of 3.5 cm), the gravitational force could be high enough to give rise to a considerable additional convective flux. However, their experiments in narrow channels (distance between membranes of 1 mm) showed that the essential increase of salt ion fluxes in the overlimiting current region in the course of dilute solutions must be produced by mechanisms other than gravitational convection.[9] Also, the orientation of the membrane system in the Earth's gravitational field had no influence on the current transport.

Rubinstein et al.[24−26] neglected the influence of gravitational convection by a simple calculation. Gravitational instability of a laminar sublayer at a smooth solid/liquid interface in a well-mixed bulk flow can occur only under certain hydrodynamic conditions. It will destroy a horizontal diffusion layer with a positive upward density gradient only if the respective Rayleigh number is greater than 1000. For diffusion layers of 0.001 or 0.1 M NaCl solutions with thicknesses of 200 μm or less, the Rayleigh numbers are 11.6 and 116, respectively. These values are at least 1 order of magnitude lower than the instability threshold.

Krol et al.[8] investigated the influence of the gravitational force by chronopotentiometric measurements of ion-exchange membranes in different cell configurations (see Figure 4). They found that, when the membrane was in the horizontal position (Figure 4b), gravitation stabilized the concentration gradient in the laminar boundary layer. The occurrence of natural convection was minimized, allowing the concentration profile to grow into the solution in time. In fact, this led to the conclusion that gravitational convection contributes to the overlimiting current. However, it is unlikely to be the origin. Large fluctuations in voltage drop were found even when the membrane was in a horizontal position and no solution flow was applied (Figure

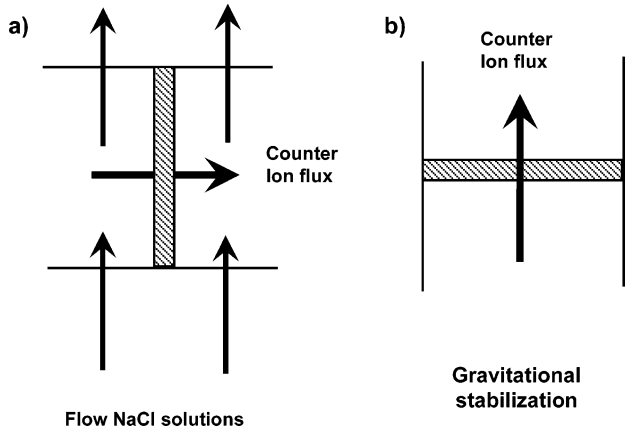

Figure 4. Schematic drawing of the membrane arrangements used in chronopotentiometry. (a) The test membrane is in the vertical position, and solution flow through the cell is applied. (b) The test membrane is in a horizontal position, and no solution flow is applied.

4b), and the depleted diffusion layer was stabilized by gravitation. Therefore, these fluctuations must represent hydrodynamic instabilities and convection of a type other than gravitational. All of the discussion above indicates that gravitational convection is most likely not the origin of the overlimiting current but contributes once destabilization of the laminar boundary layer has set in.

Electroconvection. Rubinstein and co-workers[21,24−30] explored the physical origin of enhanced transport in the overlimiting current region and elaborated the theory of electroconvection as a phenomenon that destabilizes the hydrodynamic boundary layer (Figure 3). Electroconvection is defined as nongravitational free convection in macroscopic domains of the electrolyte solutions, caused by the interactions of a self-consistent electric field with the corresponding space charge. The following two modes of electroconvection in strong electrolytes can be distinguished: The first is the relatively recently invoked "bulk" electroconvection, due to the volume electric forces acting on a macroscopic scale in a locally quasi-electroneutral electrolyte.[31−38] The second is the common electro-osmosis, either of the classical "first" kind or of the "second" kind, according to terminology of Dukhin and Mishchuk.[23,39] Electro-osmosis of the first kind[40−43] relates to the electrolyte slip resulting from the action of the tangential electric field on the space charge of a quasi-equilibrium electric double layer. (The notion of "induced-charge" electro-osmosis[42−44] refers to the dependence of the potential drop across a quasi-equilibrium electric double layer, governing the electro-osmotic flow rate, on the applied electric field, as opposed to the classical view in which this drop is regarded as a material constant.) Electro-osmosis of the second kind, invoked by Dukhin and co-workers,[45−48] pertains to the similar action of a tangential electric field on the extended space charge of the nonequilibrium electric double layer. In the developed stage of concentration polarization at a homogeneous permselective solid−liquid interface, such as that between an electrolyte solution and a homogeneous ion-exchange membrane, electroconvection arises as a result of instability of quiescent conduction caused by electro-osmosis of the second kind.[23] Electroconvection, developing from this instability, results in destruction of the diffusion layer, causing overlimiting conduction. Not far above the instability threshold, electroconvective vortices start oscillating in a periodic manner, resulting in the appearance of a low-frequency excess electric noise.[25]

The onset of electroconvection can be hastened by heterogeneity of the ion-exchange membrane at a suitable length scale.

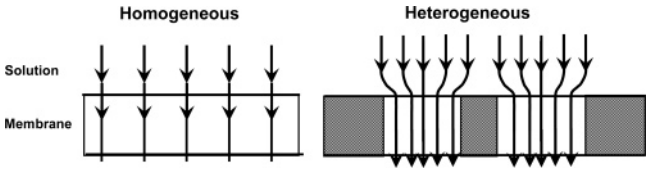

Figure 5. Scheme of the current line distribution close to homogeneous and heterogeneous membrane surfaces.

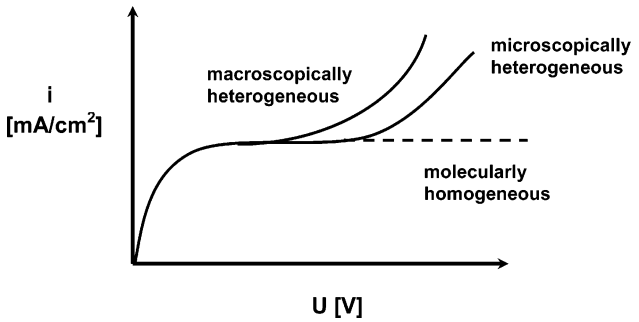

Figure 6. Dependence of the plateau length on the heterogeneity of the membrane.

Such heterogeneity is tantamount to inhomogeneous surface conductance and electric field lines concentrating in spots of higher conductance (Figure 5). In this case, the equipotential surfaces are no longer parallel to the membrane, and tangential forces appear. Flow vortices of the size typical of the surface heterogeneity result and precipitate the onset of instability, eventually causing mixing of the diffusion layer.[24] According to this concept, elimination of the electro-osmotic slip along the membrane surface should preclude the onset of electroconvection at a perfectly homogeneous flat membrane, and thus, no overlimiting conductance should occur through such a membrane (Figure 6). In fact, Rubinstein et al.[26] used a poly(vinyl alcohol) coating layer on the membrane surface (1−2 μm) to eliminate the lateral electro-osmotic slip and, thus, the overlimiting conductance.

In summary, to have an earlier onset of the overlimiting current and reduce the plateau length of the membrane's polarization curve, macroscopic heterogeneity of the membrane surface at a suitable length scale can be helpful (see Figure 6). The theoretical framework of Rubinstein et al. reveals that membrane conductive heterogeneity and surface undulation (geometrical heterogeneity) can indeed affect the plateau length (Figure 6). According to their calculations, a decrease of the plateau length would be expected if one were able to imprint surface undulations in the size range of the boundary-layer thickness.[21,24−30] Rubinstein et al. predicted that a 10% increase in the roughness of a flat surface would result in a 30% decrease of the plateau length.[25] This prediction has not yet been verified experimentally.

In this work, our research aims to design conductive and surface architecture heterogeneity affecting the overlimiting current at cation-exchange polymers. Therefore, we prepared membranes with designed inhomogeneity and tried to answer experimentally the question posed by Rubinstein et al.:[24] "can one influence polarization and local mixing of the boundary layer by designed inhomogeneity?"

2. Experimental Section

2.1. Commercial Membranes. Neosepta CMX and CMS (Tokuyama Soda Ltd., Tokyo, Japan), FT−CM (FuMA-Tech, St. Ingbert, Germany), and Nafion (Dupont) membranes were used to investigate the influence of conductive heterogeneity

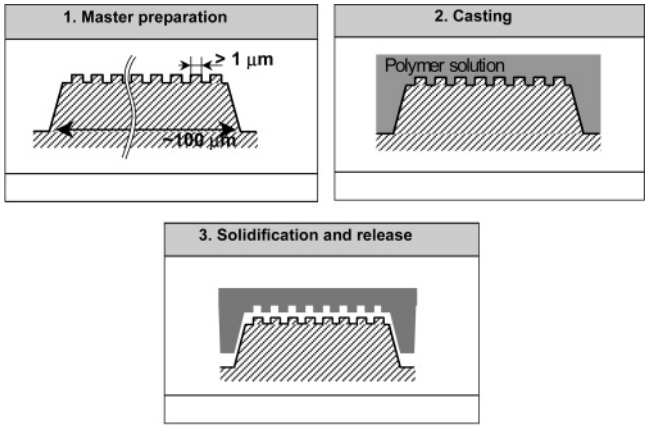

Figure 7. Preparation route of micropatterning on ion-exchange membranes. The resulting microarchitecture carries the imprint profile of the mold.

on current−voltage characteristics. Both Neosepta and Nafion are so-called homogeneous ion-exchange membranes (the polymer itself is conductive), whereas FT−CM is a so-called heterogeneous ion-exchange membrane (ion-exchange resins in a nonconductive polymer matrix).

The commercial CMX membrane was also coated with a polycation, poly(ethylenimine) (PEI), to determine the differences in surface morphology and their effects on the onset of the overlimiting current. The PEI coating was made using the following protocol: The functional membrane groups were brought into the proton form by immersing the CMX membrane in 1 M HCl solution. The solution was replaced three times in 24 h for complete exchange of functional groups. The membrane was washed in ultrapure water until the rinsewater was free of Cl^-. Then, the membrane was immersed in 0.001 wt % aqueous PEI solution (solution replaced three times, in a total of 24 h). Because of the strong electrostatic interaction between the cation-exchange membrane and the PEI, the membrane surface was covered with a thin PEI layer. The membrane was then washed with ultrapure water to remove the excess of PEI and brought back into the sodium form by immersion in 2 M NaCl solution for 24 h. The NaCl solution was replaced three times for the complete exchange of functional groups. Excess NaCl was washed away with ultrapure water for 24 h.

2.2. Tailor-made Membranes. All prepared membranes were based on sulfonated poly(ether ether ketone) (S-PEEK), which was prepared by sulfonation of poly(ether ether ketone) (PEEK, 450PF, Victrex) as described by Balster et al.[49] Different polymer solutions containing 10−20 wt % polymer in *N*-methyl-2-pyrrolidinone (NMP) were prepared, three solutions containing only S-PEEK with various sulfonation degree (SDs) and three solutions containing S-PEEK blended with poly(ether sulfone), PES: (1) 100% S-PEEK (SD 65%), (2) 100% S-PEEK (SD 75%), (3) 60% S-PEEK (SD 75%) with 40% PES, (4) 100% S-PEEK (SD 80%), (5) 80% S-PEEK (SD 80%) with 20% PES, and (6) 60% S-PEEK (SD 80%) with 40% PES.

To prepare flat films of S-PEEK and S-PEEK/PES blends, the polymers were added in the desired amounts to the solvent. After at least 24 h of stirring, the polymer solution was filtered over a 25-μm metal filter. The films were prepared by the evaporation technique.[50,51] The solutions were cast on glass plates with a 0.5-mm casting knife. The films were dried for 1 week in N_2 atmosphere at 40−80 °C, then immersed in water, and subsequently dried under vacuum at 30 °C for 1 week. The membranes were stored in 0.1 M NaCl.

Corrugated membranes were prepared by casting the polymer solution (10 and 20 wt % polymer) on a silicon-machined master wafer having patterns etched into the surface by photolithography. The process comprises three steps (Figure 7): (1) Preparation of a microstructured master mold based on technologies derived from microelectronics and photolithography, (2) casting of the polymer solution onto the master, and (3) solidification into the microsize three-dimensional microarchitecture and release from the mold.

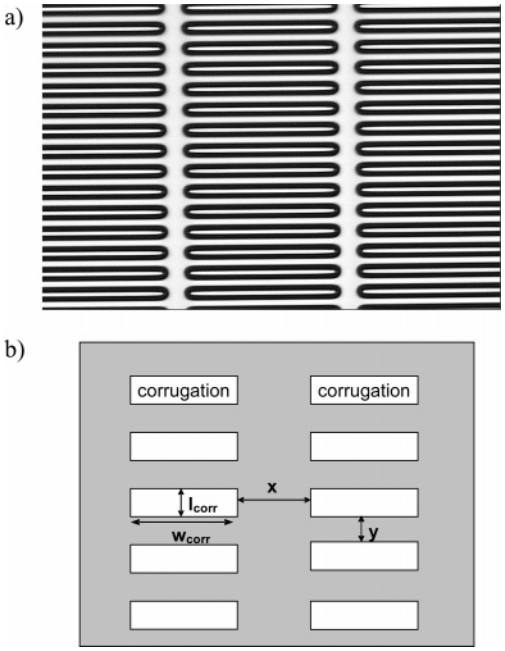

Figure 8. Schematic of mold A with dashed-line corrugation: (a) optical microscope image, (b) scheme of the corrugations at the surface.

TABLE 1: Geometrical Parameters of the Three A Molds

mold	x (μm)	y (μm)	l_{corr} (μm)	w_{corr} (μm)	depth (μm)
A1	25	50	30	360	35
A2	55	30	30	360	15−60
A3	75	50	30	360	40

The films were dried for 1 week in N_2 atmosphere at room temperature and removed from the mold by immersion in ultrapure water. Then, the films were dried as described above.

Undulated membranes with two different line structures were prepared. The first structure contained dashed lines (mold A, Figure 8a). To investigate the influence of the dimensions of the dashed lines on the overlimiting behavior, the distance between the lines was varied (see Figure 8b). The corrugations were held constant with a length of 360 μm and a width of 30 μm. The distances in the x and y directions were varied (see Table 1).

The second structure (mold B) contained continuous undulations with a width of 50 μm and a depth of 20 μm. The distance between the undulations was varied from 50 to 550 μm. A scheme of the structure of mold B is shown in Figure 9.

2.3. Membrane Characterization. The commercial and tailor-made CEMs were characterized by measurements of the ion-exchange capacity (IEC), water uptake (w), and electrical resistance (R). These properties were used to calculate the degree of sulfonation (SD) and the specific conductivity (cond) of each membrane.[49,50]

The geometrical characteristics of the molds and prepared membranes were visualized by optical microscope (Zeiss Axiovert 40 MAT) and by scanning electron microscope (Jeol JSM-T220 and JSM 5600LV). The membrane samples used for

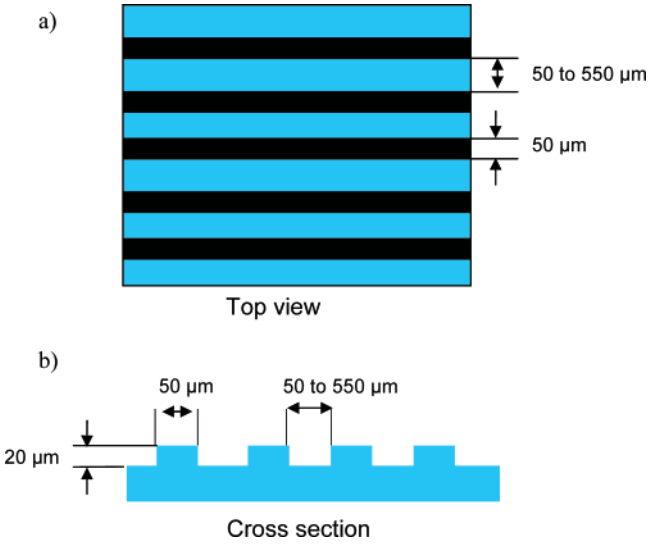

Figure 9. Scheme of the undulated mold B: (a) top view and (b) cross section.

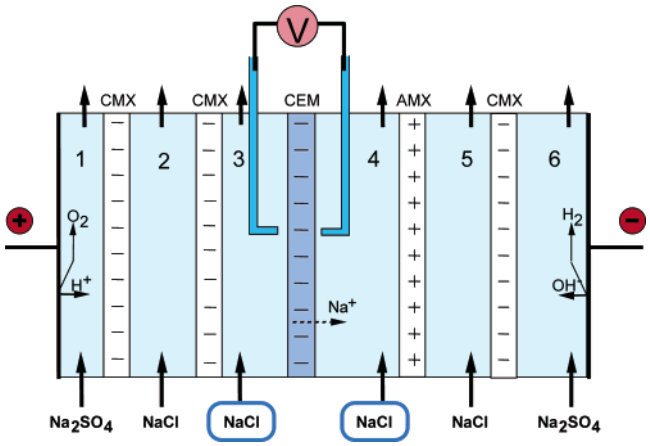

Figure 10. Six-compartment cell configuration for $i-v$ curve and chronopotetiometric measurements.

SEM were sputtered with a thin layer of gold (30 nm) using a Balzers Union SCD 040 sputtering device.

2.4. Current−Voltage and Chronopotentiometric Measurements. The $i-v$ and chronopotentiometric measurements were performed in a six-compartment cell with a four-electrode arrangement (Figure 10) under direct current using a 0.1 M NaCl solution.[7] The membrane was first equilibrated in the measurement solution for more than 24 h. The measurement solution was added to compartments 3 and 4, next to the investigated membrane with the calomel reference electrodes. In compartments 2 and 5, a 0.5 M NaCl solution was used to reduce the influence of the electrode reactions at the working electrodes. The current was applied through the working electrodes in compartments 1 and 6, whereas the electrical potential was measured close to the membrane surface in the compartments 3 and 4 with the calomel reference electrodes. The flow rate through the measurement compartments 3 and 4 was 300 mL/min.

The $i-v$ measurements are steady-state measurements. They were determined by applying a stepwise increase of the current density through the cell and recording the corresponding steady-state voltage drop values. The current density, i, follows Faraday's law and is given by

$$i = \frac{zDF(c_b - c_m)}{\delta(t^m - t^{bl})} \quad (1)$$

where t^m and t^{bl} are the transport numbers of the ion in the membrane and in the boundary layer, respectively; z is the valence of the ion; D is the diffusion coefficient of the ion; F is the Faraday constant; c_b and c_m are the concentrations in the bulk and at the membrane surface, respectively; and δ is the thickness of the boundary layer.[51] When the ion concentration at the membrane surface, c_m, approaches 0, a limiting current density, i_{lim}, is reached[51]

$$i_{lim} = \frac{zDFc_b}{\delta(t^m - t^{bl})} \quad (2)$$

The values of the limiting current density and plateau length (pl) can be determined from the measured $i-v$ curves (see Figure 2). To neglect the influence of the distance from the measurement capillaries to the membrane sample onto the $i-v$ curves, a correction for the initial ohmic resistance (R_{Ohmic}) was applied. In this case, an ohmic voltage drop that equals the ohmic resistance was subtracted from the measured value (U)

$$U_{corr} = U - iR_{Ohmic} \quad (3)$$

Figure 11 shows the $i-v$ curves of a Nafion membrane with and without the correction for the ohmic resistance.

Chronopotentiometry is an electrochemical characterization method that measures the electric potential response of a system to an imposed current. Investigation of kinetic effects, adsorption, and transport phenomena near electrode surfaces can be performed with this technique.[52−54] Chronopotentiometric measurements are dynamic measurements. A constant current density is applied, and the voltage drop between the electrode and a reference electrode is measured as a function of time. Typical examples of chronopotentiometric curves, measured with a commercial CMX membrane, are fully explained by Krol et al.[8] and Choi et al.[55] When an electric current is applied to an ion-exchange membrane system, concentration polarization phenomena arise as a result of concentration gradients formed near the membrane surface. The transient decrease of the salt concentration occurring near the membrane until a steady state is reached can be studied by measuring the voltage drop across the membrane as a function of time.[1,56] When the concentration reaches 0 at the membrane surface, the voltage rapidly increases. The time taken for the voltage transition to occur after a constant current is applied is called the transition time (τ) and is given by

$$\tau = \frac{(c_b zF)^2 \pi D}{(t^m - t^{bl})^2 4i^2} \quad (4)$$

or

$$i\tau^{1/2} = \frac{c_b zF}{(t^m - t^{bl})} \frac{(\pi D)^{1/2}}{2} \quad (5)$$

Equation 4 is equivalent to the Sand equation (eq 5) and shows that the transition time is proportional to the inverse of the square of the current density.[8,56] The transition time increases when the membrane transport number decreases, i.e., when the membrane is less selective.[1] In the overlimiting current region, only a quasi-steady-state voltage drop is reached, characterized by large fluctuations.[8] These strong fluctuations are indications

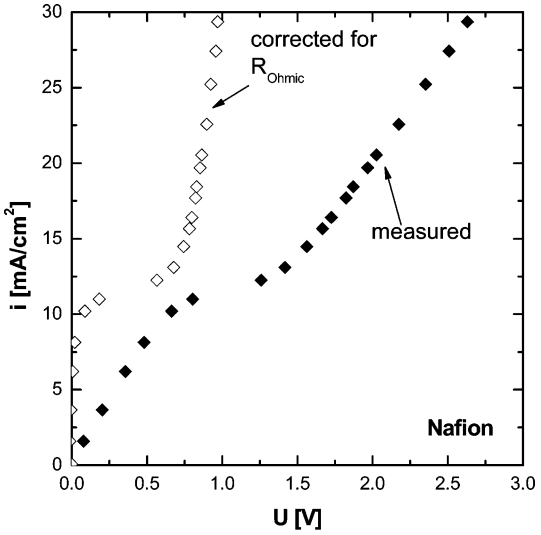

Figure 11. Measured and corrected $i-v$ curves of a commercial Nafion membrane.

TABLE 2: Plateau Lengths of Commercial Membranes

		plateau length (V)	
membrane	IEC (mol/kg_{dry})	side a	side b
CMX	1.65	0.74 ± 0.02	0.66 ± 0.02
CMS	2.09	1.14 ± 0.03	1.00 ± 0.03
Nafion	0.89	0.78 ± 0.02	0.80 ± 0.02

of the presence of hydrodynamic instabilities that occur in the depleted diffusion layer in this current region.[57,58]

The i_{lim} value determined by the $i-v$ curve measurements and the membrane selectivity determined by chronopotentiometry were used in eq 2 to calculate the thickness of the hydrodynamic boundary layer for homogeneous membranes. The chronopotentiometric measurements were also used to evaluate the conductive heterogeneity of the membranes.[8,56,59] Therefore, the experimentally determined transition times were compared with the transition times calculated for a 100% permselective membrane ($t^m = 1$).[8]

2.5. Simulation of the Solution Stream Line Distribution. To simulate the flow stream lines of the liquid along the membrane surface, COMSOL, a multiphysics finite-element analysis software, was used to numerically model the coupled flow in two dimensions at steady state. The code solves the Navier−Stokes (NS) and continuity equations for incompressible flow. Velocity field lines for a 200-μm layer along the membrane surface were calculated assuming a parabolic flow distribution, resulting in a linear flow profile at the membrane surface. The flow velocity was estimated to be 1 cm/s.

3. Results and discussion

3.1. Commercial Membranes. First, the effect of the conductive heterogeneity on the current−voltage behavior of cation-exchange membranes was investigated. Three homogeneous commercial cation-exchange membranes were used (CMX, CMS, and Nafion). The conductive heterogeneity at both sides (denoted as a and b) toward the anode was investigated (see Table 2). The plateau length was identified from the intersection points depicted in Figure 2. The errors for the plateau length can be estimated from the linear regressions performed in regions 1 and 3.[1]

The CMX and Nafion membranes have lower plateau lengths than the CMS membrane. All three membranes are microscopically heterogeneous membranes containing functionalized polymers, but they differ in their morphologies (see Figure 12). The Nafion membrane contains SO_3^- and COO^- groups and a perfluorinated polymer backbone. It has the lowest IEC of the three membranes and seems to be more heterogeneous than CMX and CMS, which contain only SO_3^- groups. The even lower plateau length of the CMX membrane is probably due to the nonconductive reinforcement inside the membrane (Figure 12a). The CMS membrane has reinforcement too, but because it is a monovalent-ion-selective membrane, it contains a thin positively charged coating layer on both sides. This coating hides

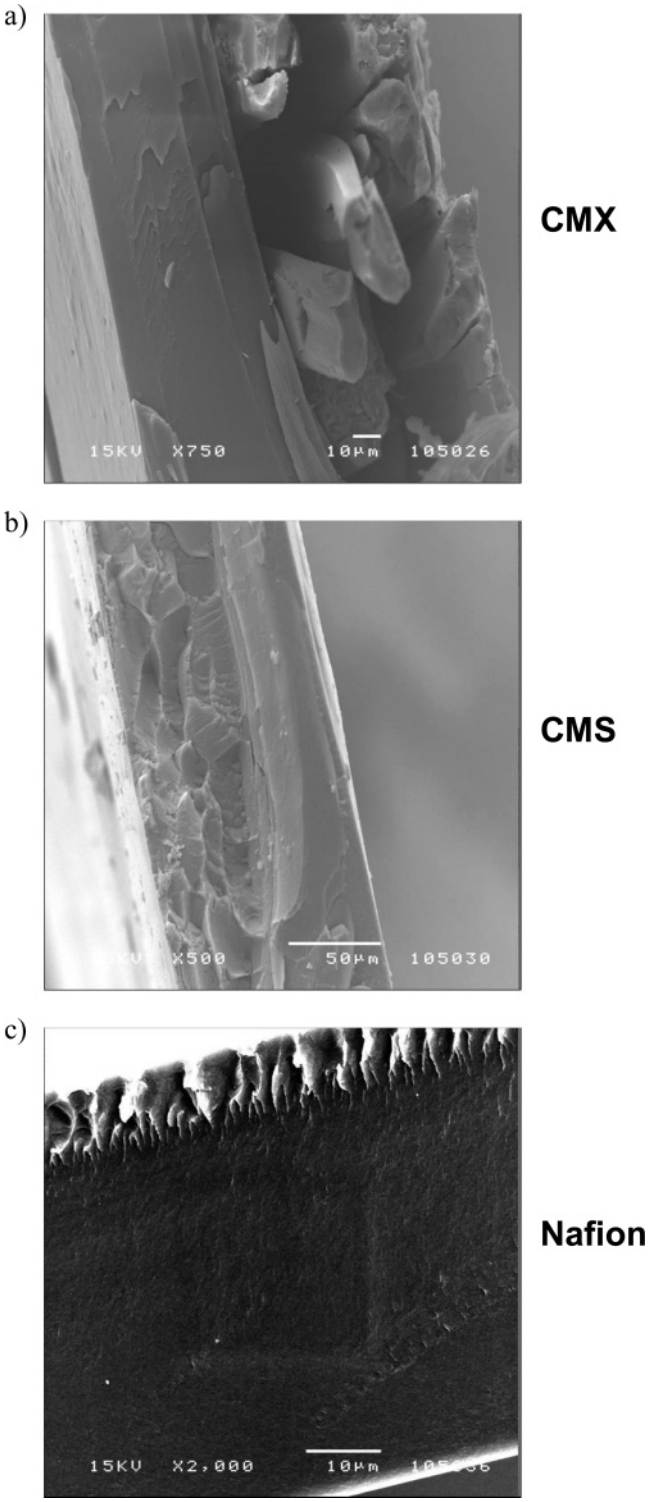

Figure 12. SEM images of the cross sections of (a) CMX, (b) CMS, and (c) Nafion membranes.

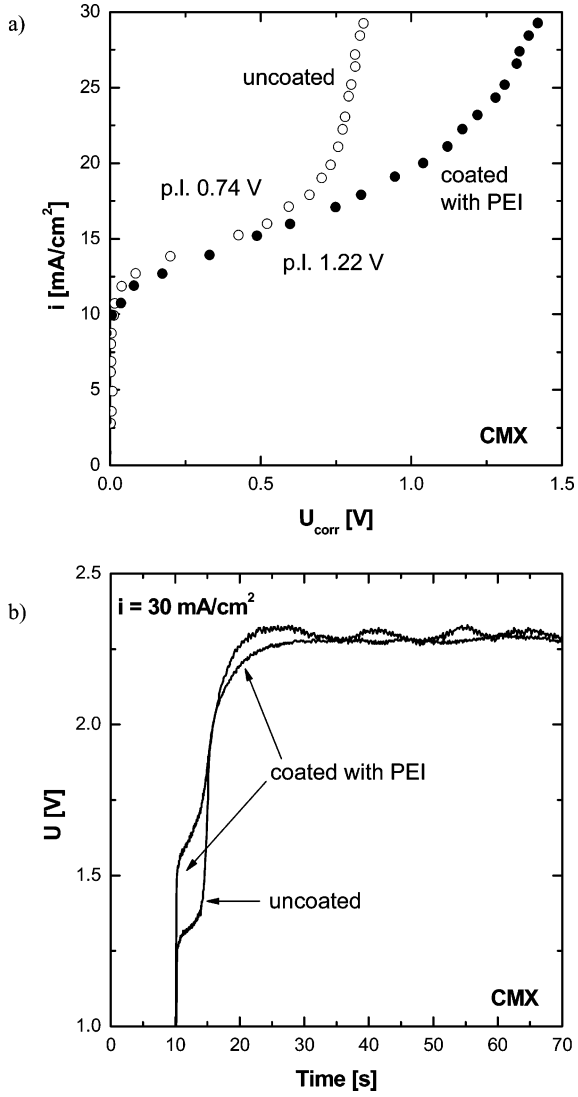

Figure 13. Comparison of the (a) $i-\upsilon$ curve and (b) chronopotentiometric measurements of a CMX membrane before and after coating with PEI, measured in 0.1 M NaCl.

TABLE 3: Plateau Lengths of the CMX Membrane before and after the PEI Coating

	plateau length (V)			
	side a		side b	
membrane	initial	coated	initial	coated
CMX	0.74 ± 0.02	1.22 ± 0 02	0.66 ± 0.02	1.18 ± 0.02

membrane surface heterogeneities and results in a longer plateau length compared to those of the other two membranes (Table 2). In contrast to the CMX and CMS membranes, the unreinforced Nafion membrane does not show significant differences between the plateau lengths of the two membrane sides.

To obtain better insight into the influence of the surface morphology of a membrane on the plateau length and the overlimiting current, the CMX membrane was coated with a thin PEI coating (as described in section 2.1). A comparison of the $i-\upsilon$ curves (Figure 13a, corrected for the ohmic resistance) and the chronopotentiometric measurements (Figure 13b, not corrected) of coated and uncoated CMX samples shows the different behavior of the membranes. The plateau length of the coated CMX membrane is higher than that of the uncoated one, and it is the same for both membrane sides (Table 3). The overlimiting current appears at a higher potential. In addition,

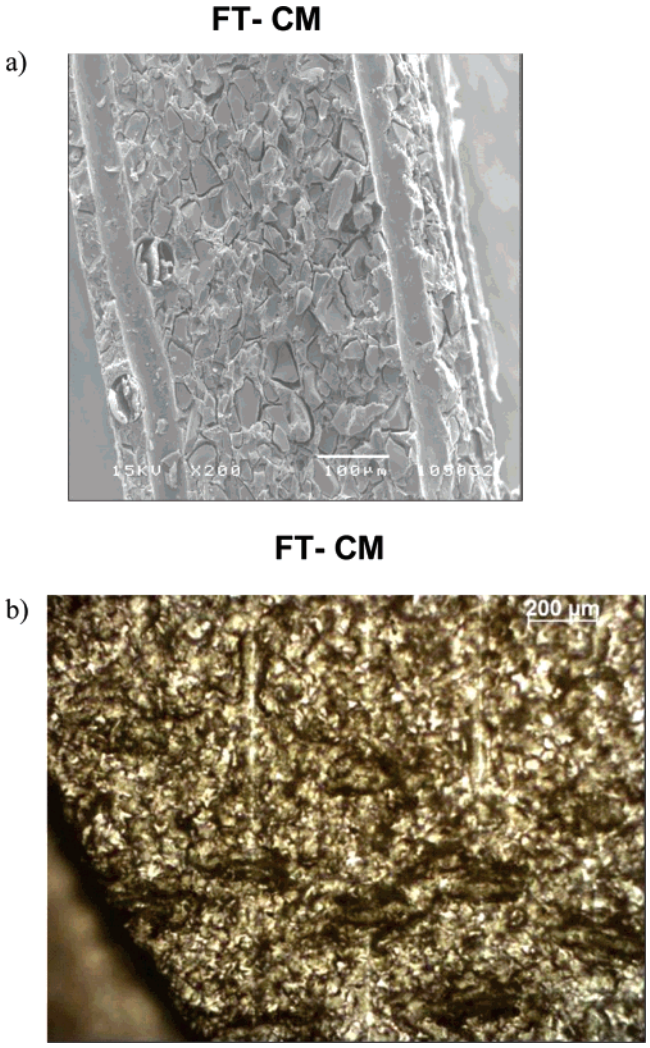

Figure 14. Heterogeneous FT−CM membrane: (a) SEM image of the cross section and (b) surface image obtained with an optical microscope.

the slope of the current increase with voltage drop in the overlimiting current region is not as steep, indicating a higher resistance for the coated membrane (Figure 13a). The chronopotentiometric measurement shows that the voltage instabilities in the overlimiting region are lower for the coated membrane (Figure 13b). This indicates that the PEI coating on the CMX membrane leads to decreased hydrodynamic instabilities. The coating hides the surface heterogeneity and results in a later occurrence of the overlimiting current, but does not eliminate it. These experiments are consistent with the findings of Rubinstein et al.,[26] who reported the shifting and even elimination of the overlimiting conductance by poly(vinyl alcohol) coatings of 1−2 μm.

3.2. Heterogeneous vs Homogeneous Commercial Ion-Exchange Membranes. After the investigation of the commercial homogeneous membranes (microscopically heterogeneous), we investigated the influence of the membrane surface heterogeneity on the $i-\upsilon$ curves of the FT−CM membrane, a reinforced heterogeneous cation-exchange membrane (macroscopically heterogeneous, Figure 14). Images of the cross section (Figure 14a) and the surface (Figure 14b) show the heterogeneity of the FT−CM membrane, which contains ion-exchange particles of different sizes and shapes glued together by a nonconductive polymer.

Chronopotentiometric and $i-\upsilon$ curve measurements with the heterogeneous FT−CM membrane were performed, and the

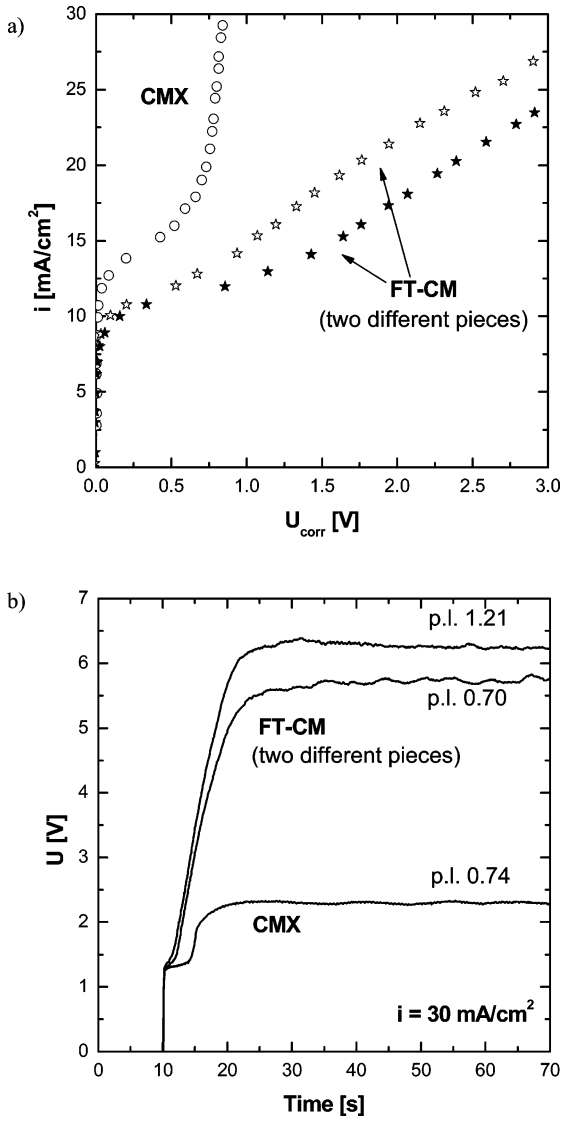

Figure 15. Comparison of the (a) $i-\upsilon$ curve and (b) chronopotentiometric measurements of the CMX and of two different pieces of the FT−CM membrane, measured in 0.1 M NaCl.

results were compared with those for the homogeneous CMX membrane (Figure 15). The comparison of the $i-\upsilon$ curves (Figure 15a) corrected for the total ohmic resistance shows significant differences between the two membranes. The resistance of the heterogeneous FT−CM membrane is higher in the overlimiting region than the resistance of the homogeneous CMX membrane. The plateau length of the FT−CM membrane varies strongly and depends on the piece of the film that was investigated (plateau lengths from 0.70 to 1.21 V were measured). The chronopotentiometric measurements show that the transition times of the FT−CM membrane are much lower than those of the CMX membrane (Figure 15b). It is interesting to note that the FT−CM membrane sample with the shortest plateau length (0.70 V) shows the strongest fluctuations in voltage drop in the overlimiting region, indicating the presence of hydrodynamic instabilities in the boundary layer. In this case, the overlimiting current probably sets in earlier because of electroconvection induced by the heterogeneity of the membrane sample.

A reason for the difference in plateau length between the FT−CM membrane samples might be the influence of the reinforcement of the membrane, which is not homogeneously distributed over the membrane surface (see Figure 16) and therefore

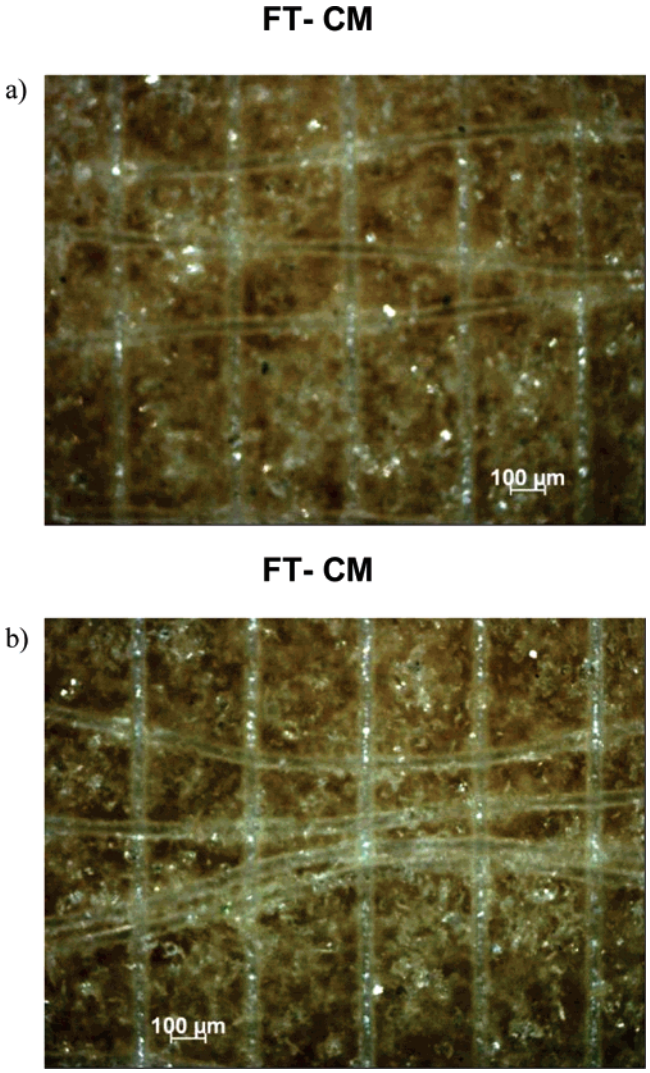

Figure 16. Images of the surface of different pieces of the FT−CM membrane.

changes the heterogeneity of the membrane surface. In some samples, the distance between the nonconductive fibers of the FT−CM membrane was greater than 200 μm, which is in the range of the hydrodynamic boundary layer. According to Rubinstein et al.,[21,24−30] shortening of the plateau length occurs if the heterogeneities have a size on the order of the magnitude of the boundary-layer thickness. This could explain the earlier initiation of the overlimiting current for these samples.

The heterogeneous nature of the FT−CM membrane can also be seen by plotting $i\tau^{1/2}$ as a function of the applied current density and comparing the plots with those calculated for membranes with different permselectivities (100% and 90%, see Figure 17). The $i\tau^{1/2}$ values were calculated according to eq 5, using a NaCl diffusion coefficient of 1.48 m^2/s and a Na^+ solution transport number of 0.39 (values for a 0.1 M NaCl solution).[60] The experimentally determined transition times of the CMX membrane are higher than those of a 100% permselective membrane, showing a homogeneous electrical field line distribution. Therefore, the permselectivity of the CMX membrane can be calculated using the Sand equation. The heterogeneous FT−CM membrane shows lower transition times than a 100% permselective membrane. This difference confirms that the membrane contains an inert ion-impermeable region. The reduced ion-permeable area of the FT−CM membrane corresponds to a locally higher current density at the points where the membrane is conductive (see Figure 5), causing a faster salt

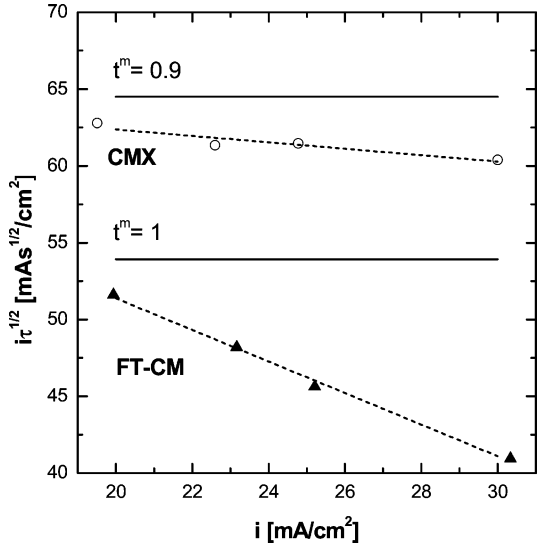

Figure 17. Comparison between experimental and calculated $i\tau^{1/2}$ values for the CMX membrane, the FT−CM membrane, a 100% permselective membrane ($t^m = 1$), and a 90% permselective membrane ($t^m = 0.9$).

depletion near the membrane. Therefore, lower transition times are observed because the entire membrane area is not available for ion conduction.[56] Because the current is normalized for the overall membrane area, impermeable areas have to be taken into account to avoid underestimation of current densities.

The results presented above show that the surface heterogeneity of the membrane influences the plateau length and the overlimiting current. The results for the FT−CM membrane show that conductive heterogeneity can shorten but also prolong the plateau length of the membrane, depending on the distance between the surface heterogeneities. Both cases have been reported by other researchers as well.[1,56,61]

3.3. Homogeneous Blend Membranes. To tailor the conductive heterogeneity of the membranes, tailor-made cation-exchange membranes using S-PEEK of various degrees of sulfonation and S-PEEK/PES blends were prepared and investigated. The errors of the initial measurements were estimated by linear regression performed in regions 1 and 3 of the $i-v$ curve (Figure 2). The error for the equilibrated membranes is the standard deviation of the plateau lengths of the corresponding side measured over 6 weeks after the initial measurement.

Figure 18 shows the measured plateau lengths of two tailor-made membranes over time. For the pure S-PEEK membrane (SD 80%), the plateau length of the air side increases significantly over time, whereas the plateau length of the glass side increases much less (see Figure 18a), in agreement with earlier studies.[1] The same effect can be seen with pure S-PEEK membranes of lower sulfonation degrees (see Table 4). With increasing membrane sulfonation degree, the difference between the initial plateau lengths of the air side and the glass side decreases. The plateau length of the air sides in the equilibrated state increases with increasing sulfonation degree, whereas it stays constant for the glass sides, within the experimental error. The development of the plateau length of the S-PEEK/PES blends is different (Figure 18b). For both sides, it increases with time and reaches the same value at equilibrium (see Table 4).

It seems that the membrane sides obtain different surface heterogeneities during the drying process, as explained by Ibanez et al.[1] These heterogeneities are not stable over time. The membranes are stored in solution, which allows the polymer matrix to swell. Because the membranes are in a hydrophilic

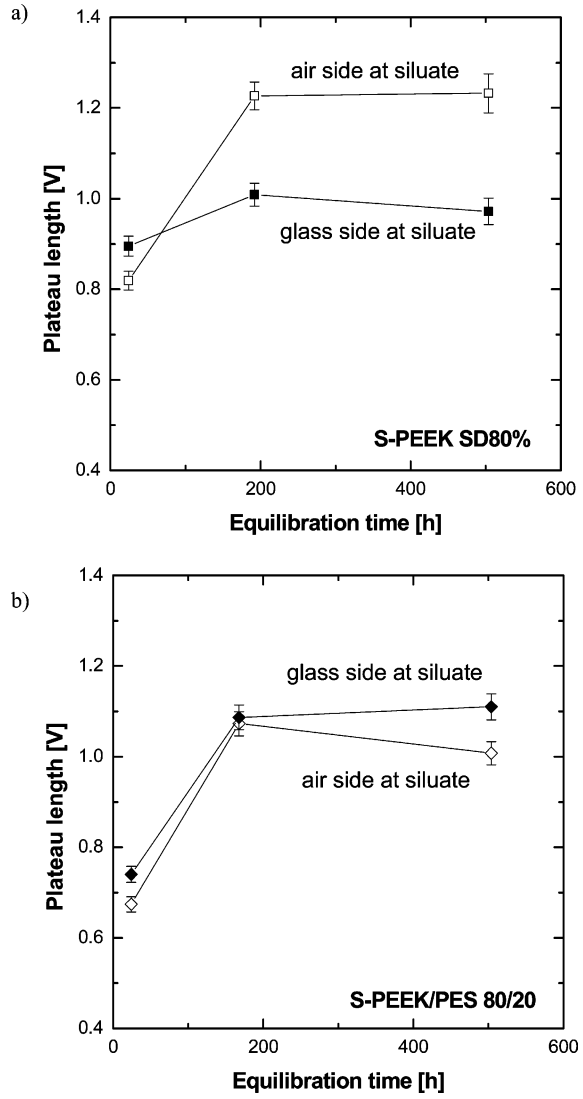

Figure 18. Effect of the equilibration time on the plateau length of (a) an S-PEEK membrane with a sulfonation degree of 80% and (b) an S-PEEK/PES 80/20 blend membrane (S-PEEK SD 80%).

environment, the polymer structures relax to reduce the surface energy and entropy of the system. Therefore, the hydrophilic groups of the polymer (SO_3^- groups) will orient toward the surface of the membrane and give a more homogeneous conductivity.

An indication of this phenomenon is shown by the development of the transition times over time (see Table 5). The $i\tau^{1/2}$ values of the prepared membranes increase over time. Because no loss of permselectivity is found (the limiting current densities stay constant over time and are the same for both sides), these changes can only be due to changes in heterogeneity. The transition times are all higher than those for a 100% permselective membrane, indicating a low amount of inert, ion-impermeable regions and, therefore, a quite homogeneous electrical field line distribution. For the initial measurements, a lower sulfonation degree and a higher amount of PES result in lower plateau lengths and lower transition times, especially for the air sides of the membranes. After equilibration, these differences are minimized. For the specific system under study (S-PEEK/PES), it seems that the variation of sulfonation and blending cannot introduce sufficient permanent conductive heterogeneity to induce electroconvection.

In conclusion, our results show that the conductive heterogeneity of an ion-exchange membrane influences the occurrence

TABLE 4: Comparison of the Initial Plateau Length and the Average Plateau Length Developed over Time (6 Weeks) for the Tailor-made Membranes

	plateau length (V)			
	air side		glass side	
membrane	initial	equilibrated	initial	equilibrated
100% S-PEEK (SD 65%)	0.71 ± 0.02	0.88 ± 0.13	0.93 ± 0.03	0.99 ± 0.09
100% S-PEEK (SD 75%)	0.73 ± 0.02	0.96 ± 0.06	0.89 ± 0.02	0.93 ± 0.05
100% S-PEEK (SD 80%)	0.82 ± 0.02	1.15 ± 0.13	0.90 ± 0.02	0.94 ± 0.07
80% S-PEEK (SD 80%)/20% PES	0.67 ± 0.02	1.05 ± 0.05	0.74 ± 0.02	1.08 ± 0.16
60% S-PEEK (SD 80%)/40% PES	0.58 ± 0.02	0.97 ± 0.15	0.75 ± 0.02	1.07 ± 0.05

TABLE 5: Development of the $i\tau^{1/2}$ Values for the Tailor-made Membranes over Time: Initial vs Equilibrated Values

	$i\tau^{1/2}$ (mA s$^{1/2}$/cm^2)			
	air side		glass side	
membrane	initial	equilibrated	initial	equilibrated
100% S-PEEK (SD 65%)	59.3 ± 0.8	63.0 ± 1.7	60.1 ± 0.8	63.8 ± 1.0
100% S-PEEK (SD 75%)	62.7 ± 1.2	64.5 ± 1.5	62.8 ± 1.1	65.1 ± 1.2
100% S-PEEK (SD 80%)	65.4 ± 0.8	66.0 ± 1.0	64.3 ± 1.8	63.7 ± 1.3
80% S-PEEK (SD 80%)/20% PES	61.8 ± 1.1	63.3 ± 1.0	61.4 ± 1.0	62.7 ± 1.1
60% S-PEEK (SD 80%)/40% PES	59.8 ± 0.6	61.0 ± 0.7	59.0 ± 0.6	60.5 ± 0.7

of the overlimiting current density. An increased heterogeneity leads to smaller plateaus for the specific system. For the specific S-PEEK/PES polymer, the required conductive heterogeneity cannot be introduced by blending or using different degrees of sulfonation. The investigation of the heterogeneous FT−CM membrane showed that this heterogeneity leads to a strong decrease of the transition times through the reduced ion-permeable area of the membrane. The plateau length can decrease if the heterogeneities are in the range of the boundary-layer thickness, indicating that a certain order in this heterogeneity is necessary to allow the buildup of electroconvective vortices in a quasi-steady state.

3.4. Effect of Geometrical Heterogeneity. To confirm the prediction of Rubinstein et al.[21,24−30] that a surface undulation shortens the plateau length, microengineered membranes were prepared using mold A (Figure 8). Images of a corresponding membrane structure are shown in Figure 19.

First, mold A1, with dimensions $x = 25\ \mu$m and $y = 50\ \mu$m and a depth of 35 μm, was used for the membrane preparation. The membrane was placed in the measurement cell in two different positions (see Figure 20). In the first position, the undulation was parallel to the flow direction (Figure 20a). In the second position, the undulation was perpendicular (turned 90°) to the flow direction (Figure 20b).

Figure 21 shows the plateau length of a pure S-PEEK (SD 80%) membrane cast on mold A1 (see Table 1). Compared to the glass side of a flat membrane, the corrugation of the membrane leads to a decrease of the plateau length by 16% if the corrugation is placed parallel to the flow direction (as shown in Figure 20a). When the same membrane is turned by 90° (as shown in Figure 20b), the plateau length increases by about 30% compared to that of a flat membrane, because of an increased boundary-layer thickness.

Figure 22 shows the velocity field line distribution of the liquid flow over the membrane surface obtained by a COMSOL simulation using the geometrical parameters of the membrane surface assuming a parabolic flow distribution inside the cell. When the flow is parallel to the membrane undulation, as shown in Figure 20a, the flow goes inside the membrane undulations (Figure 22a). In contrast, a stagnant solution layer in the undulations is formed (Figure 22b) when the membrane undulations are placed perpendicular to the flow, as shown in Figure 20b. Then, the thickness of the desalinated boundary

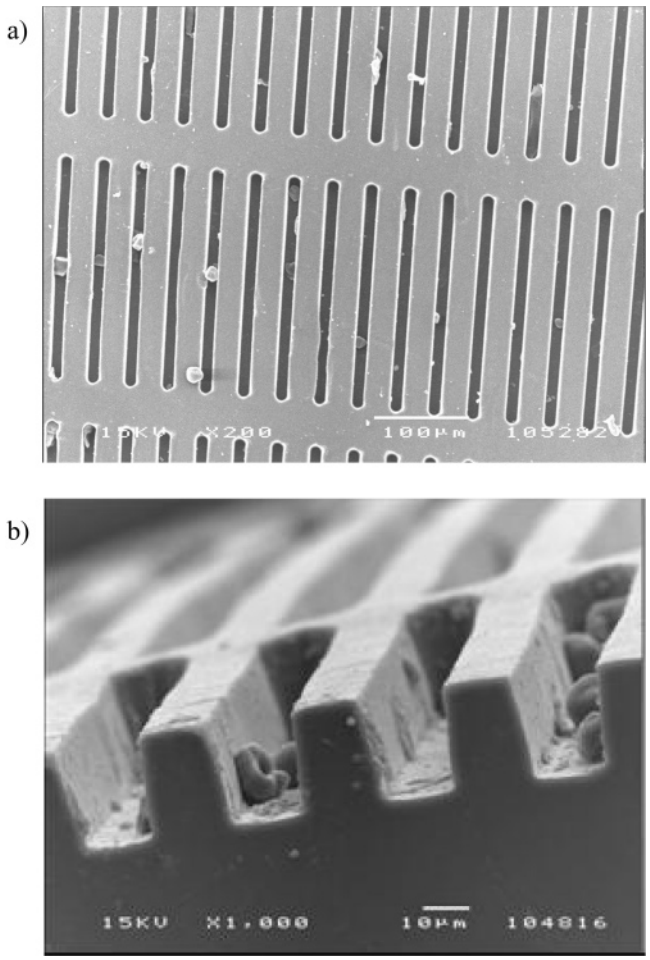

Figure 19. SEM images of the (a) surface and (b) cross section of one of the S-PEEK membranes.

layer increases in comparison to that for the flow of Figure 20a and also in comparison to that for a flat membrane.

To study the influence of the gravitational force, the corrugated membrane described above (prepared with mold A1) was placed into the measurement cell with the corrugations at the diluate side normal to the flow (Figure 20a), but in a horizontal position (see Figure 4b), and a solution flow was applied. Figure 23 shows the $i-v$ curves of two horizontal

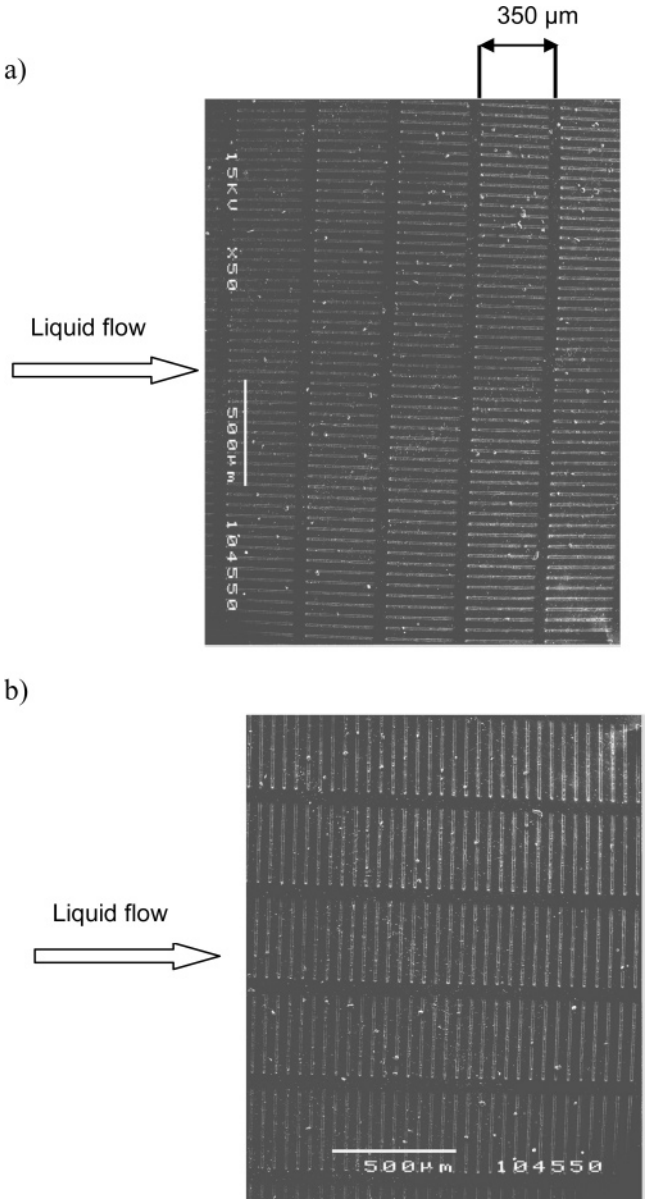

Figure 20. Scheme of the different positions of the membrane corrugation with respect to the liquid flow.

measurements in comparison to the measurement in the vertical position (see Figure 4a).

The measurement of the undulated membrane in the horizontal position shows that gravitation stabilizes the boundary layer if the diluate is at the bottom side of the membrane. The diluted boundary layer grows into the solution over time, so that no overlimiting conductance is achieved (in agreement with Krol et al.[8]). If the diluate is on top of the membrane, a plateau length similar to that obtained when the membrane is placed in the vertical position is found. Therefore, the gravitational force is most likely not the origin of the overlimiting current, but gravitational forces contribute to the destabilization as initiated by electroconvection.

To gain better insight into the influence of the geometrical parameters of the surface undulation of the membrane on the plateau length, a series of membranes was prepared using mold A2. The geometrical parameters of these molds were $x = 55$ μm and $y = 30$ μm, and the depth was varied from 15 to 60 μm (see Table 1). The membranes were prepared from two different materials: S-PEEK (SD 75%) and S-PEEK/PES 60/40 using the same S-PEEK (SD 75%). Figure 24 shows the

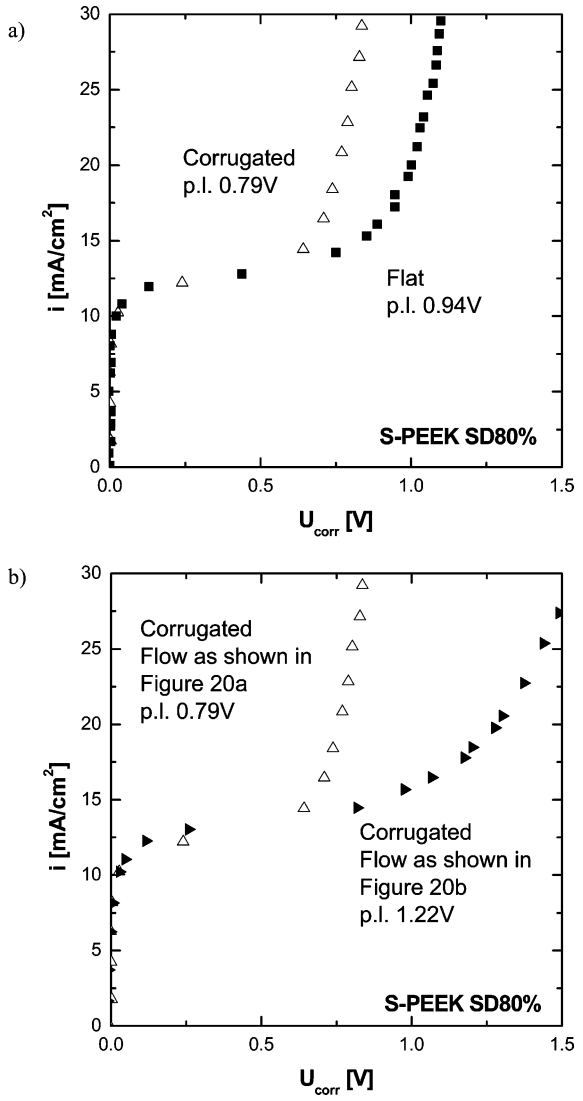

Figure 21. Comparison of the $i-v$ curves of (a) a flat membrane and a corrugated membrane oriented with respect to the flow as shown in Figure 20a and (b) the corrugated membranes with a different orientation with respect to the liquid flow.

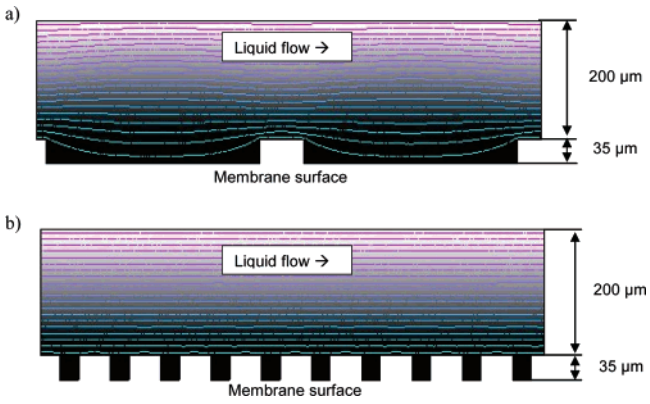

Figure 22. Velocity field lines of the liquid flow along the membrane surface simulated for a 200-μm layer on top of the membrane surface: surface corrugations (a) parallel and (b) perpendicular to the liquid flow.

plateau length determined by $i-v$ curve measurements in 0.1 M NaCl versus the depth of the molds (measured by SEM).

The plateau length of the membranes decreases significantly at higher depths. This effect is stronger for the S-PEEK/PES blends than for the pure S-PEEK membranes. The membranes containing only S-PEEK swell 3 times more in solution than

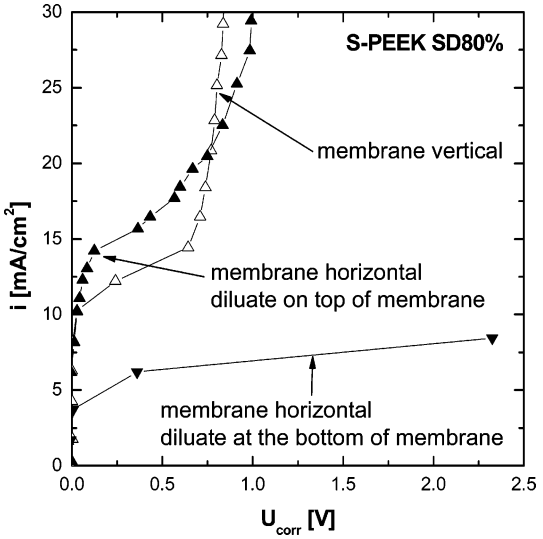

Figure 23. Comparison of the $i-v$ curves of the undulated S-PEEK (SD 80%) membrane (mold A1) measured in different positions.

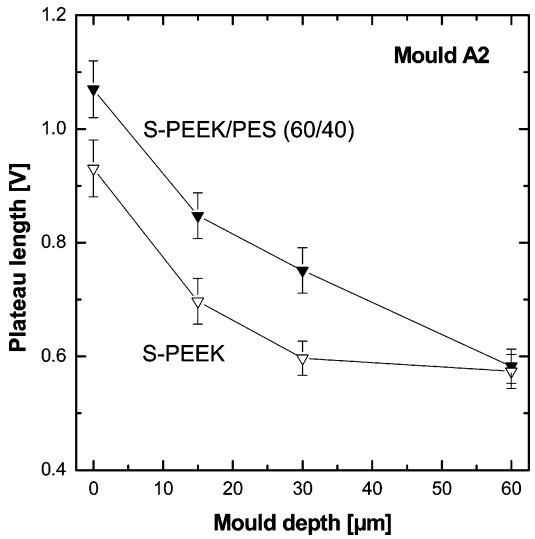

Figure 24. Plateau lengths of the S-PEEK and S-PEEK/PES blend membranes vs the mold depth (mold A2).

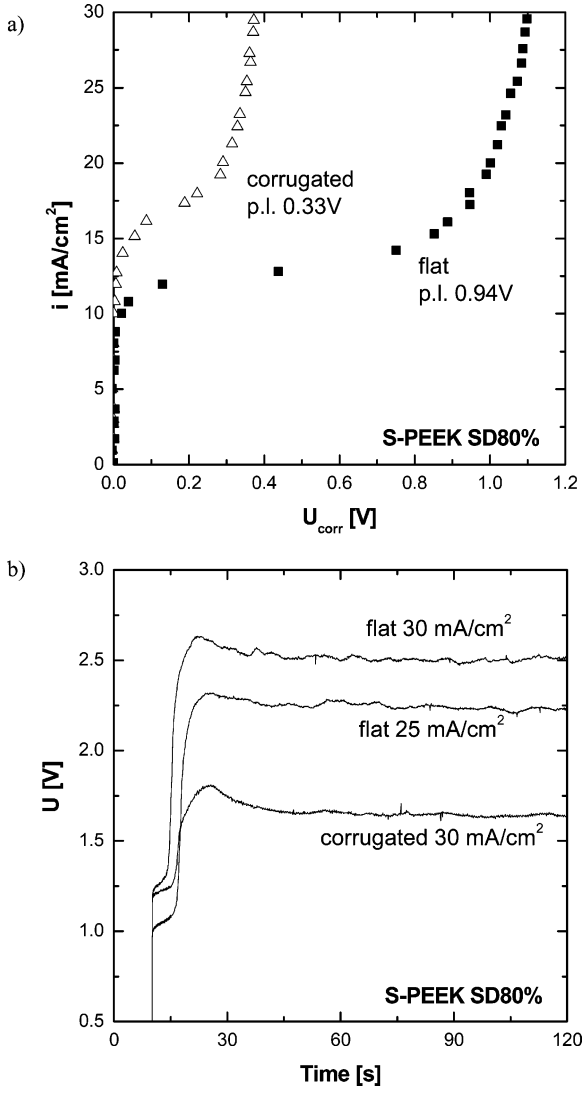

Figure 25. Comparison of the corrugated ($x = 75$ μm, $y = 50$ μm, depth $= 40$ μm, (mold A3) and flat S-PEEK (SD 80%) membranes in terms of (a) $i-v$ curves and (b) chronopotentiometric curves.

those containing S-PEEK/PES.[49] The high swelling degree of the S-PEEK membrane might result in deformation and/or reduction of the depth of the membrane undulation in comparison to the less swollen S-PEEK/PES membrane, especially at higher mold depths.

Compared to the membrane prepared with mold A1, the increase of the x distance from 25 to 55 μm decreases the plateau length of the membrane as well. This indicates that, in the case of mold A, the small line structure parallel to the flow does not cause the earlier occurrence of electroconvection. It seems that the lines separating the small corrugations normal to the flow direction are responsible for the destabilization of the hydrodynamic boundary layer. These lines are placed at a distance of 350 μm, which is the length of the small corrugations, and their thickness depends on the x value of the mold (see Figure 8b).

To obtain better insight into the influence of the thickness of the lines normal to the flow, an S-PEEK (SD 80%) membrane was prepared with mold A3 (with an increased x distance of 75 μm, see Table 1). Therefore, the thickness of the lines normal to the flow increased from 55 to 75 μm compared to the membrane prepared with mold A2. The depth of the mold was 40 μm. This increase of the thickness of the lines normal to the liquid flow leads to a tremendous decrease of the plateau length of the corrugated membrane (see Figure 25a). The resistance of the membrane in the overlimiting region is the same as in the ohmic region if the voltage drop caused by the plateau length is neglected. The limiting current density of the corrugated membrane is higher than that of a flat membrane. This is probably due to a lower permselectivity and a higher surface area of this membrane compared to a flat one. The undulated membrane was cast with the same casting knife (0.5 mm) as the flat membrane. Because of the 40-μm-deep undulations, the selective layer is much thinner than that for the flat membrane, which leads to a selectivity loss using this highly sulfonated polymer. In addition, the undulated membrane has an increased surface area (ca. 7%, estimated by the difference in i_{lim} between air and mold sides of the undulated membrane), for which the current density was not corrected.

The chronopotentiometric curves in Figure 25b present the voltage accumulation over time of the corrugated membrane compared to a flat membrane. The fluctuations in the overlimiting current region indicate the presence of electroconvection as the cause for the overlimiting current for both membranes. The transition time of the corrugated membrane is higher than that of the flat membrane because of the decreased permselectivity and increased membrane area. The transition times of the

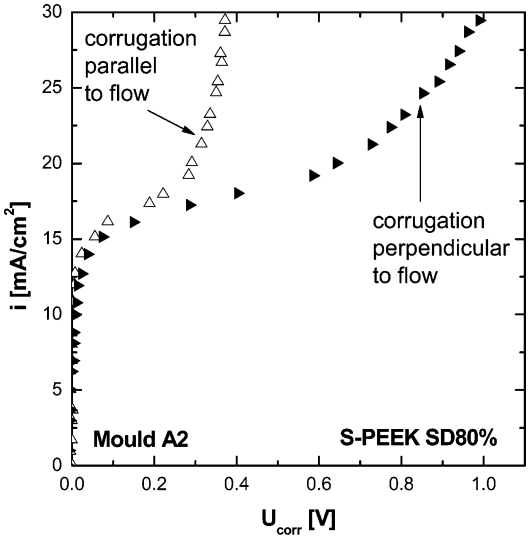

Figure 26. Comparison of the $i-v$ curves of the corrugated membrane (mold A3) with different orientations of the undulations with respect to the liquid flow.

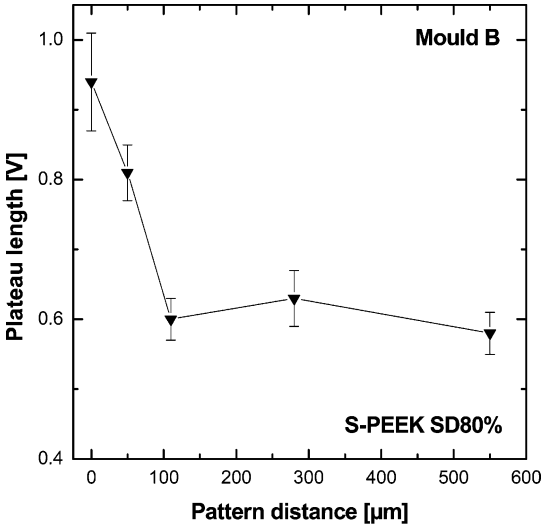

Figure 27. Comparison of the plateau lengths of a flat membrane and corrugated membranes with different distances between the lined corrugations (mold B). The lines were placed perpendicular to the liquid flow.

air and mold sides of the undulated membrane are the same, taking the increased surface area of the mold side into account. Because the membranes were prepared with pure S-PEEK (SD 80%), the membrane material is completely homogeneous, as seen before. The earlier onset of the overlimiting conductance of the undulated membrane compared to the flat membrane can therefore only be due to points of locally higher current density as a result of the geometrical undulation of the membrane surface. These points seem to appear after the buildup of the diluted boundary layer. The distance between these points is in the right order to enhance the buildup of electroconvective vortices oscillating at the membrane surface, destroying the diffusional boundary layer. Turning this membrane by 90° (as shown in Figure 20b) destroys this effect and results in a longer plateau length (see Figure 26). It seems that the small geometrical undulations increase the boundary-layer thickness because of a stagnant solution layer (see Figure 22).

According to Rubinstein et al.,[25] a periodic distortion on the length scale of the diffusion layer thickness should lead to the earlier onset of overlimiting conductance through electroconvection. The boundary-layer thickness of an S-PEEK (SD 80%) membrane in our system was determined between 230 and 250 μm. The distance between the lines separating the small corrugations normal to the flow was 350 μm (mold A, Figure 8). Our measurements thus indicate the validity of this theory.

To investigate the influence of the distance between the lines, molds like that described in Figure 9 (mold B) were used. Membranes with lines normal to the flow (50 μm wide) were prepared with the distance of the lines varied from 50 to 550 μm. The depth of mold B was 20 μm, and the membranes were prepared of pure S-PEEK (SD 80%). Figure 27 shows that a distance of 100 μm between the lines is sufficient to reduce the plateau length of the membrane significantly. A further increase of the distance to 550 μm does not show further improvement.

In conclusion, it seems that the geometrical heterogeneity has a significant influence on the onset of the overlimiting current. Creating line undulations on the membrane surface having distances in the range of approximately 50−200% of the boundary-layer thickness normal to the flow leads to an earlier onset of the overlimiting current. By increasing the height of the undulations, the effect can be enhanced. The theory of Rubinstein et al.[21,24−30] predicts a shortening of the plateau length if undulations in the size range of the boundary-layer thickness are introduced onto the membrane surface. Our measurements support the prediction of Rubinstein et al.'s theory and allow us to conclude that electroconvection seems to be the origin of the overlimiting current under the experimental conditions of this study.

4. Conclusions

The investigation of commercial cation-exchange membranes has shown the influence of the surface heterogeneity on the plateau length. The coating of a commercial CMX membrane led to a strong increase of the plateau length and a later occurrence of the overlimiting current density. The investigation of the heterogeneous cation-exchange membrane FT−CM showed that the heterogeneity reduces the transition times of the membrane because of the concentration of the electrical field lines, but that this phenomenon does not directly result in an earlier onset of the overlimiting current. The surface heterogeneities have to be at a distance in the range of the boundary-layer thickness to lead to an earlier onset of the overlimiting current.

The conductive heterogeneity obtained by using polymers of different degrees of sulfonation or by blending with nonconducting polymer did not show any long-term effect for the chosen S-PEEK/PES system.

However, the surface undulations had a significant influence on the occurrence of the overlimiting current and the earlier onset of electroconvection. In fact, line undulations on the membrane surface normal to the flow direction, having distances in the range of approximately 50−200% of the boundary-layer thickness, led to an earlier onset of the overlimiting current. By increasing the height of the undulations, the effect was enhanced. The plateau length of the undulated membranes could be reduced by up to 60% compared to that of a flat membrane.

The theory of Rubinstein et al.[21,24−30] predicts a shortening of the plateau length if undulations are within the same range as the boundary-layer thickness. Our measurements are consistent with this theory. Electroconvection is therefore most likely the origin of the overlimiting current under the conditions used in this study.

Acknowledgment. This CW/STW project was financially supported by The Netherlands organisation for scientific research (NWO). The authors thank Isaak Rubinstein for fruitful discussions.

List of Symbols

c_b = concentration in the bulk (mol/L)
c_m = concentration at the membrane surface (mol/L)
cond = conductivity (mS/cm)
D = diffusion coefficient (m^2/s)
F = Faraday constant (96485 A s/mol)
i = current density (A/m^2)
IEC = ion-exchange capacity (mol/kg_{dry})
i_{lim} = limiting current density (A/m^2)
J_{lim} = limiting flux [$mol/(m^2\ s)$]
l_{corr} = length of the corrugation (μm)
pl = plateau length (V)
R = area resistance ($\Omega\ cm^2$)
R_{Ohmic} = Initial ohmic area resistance ($\Omega\ cm^2$)
SD = sulfonation degree (%)
t^{bl} = ion transport number in the boundary layer
t^m = ion transport number in the membrane
w = water uptake (kg_{water}/kg_{dry})
w_{corr} = width of the corrugation (μm)
x = distance between the rows containing small corrugations (μm)
y = distance between the small corrugations (μm)
z = valence of the ion
NMP = *N*-methyl-2-pyrrolidinone
PEEK = poly(ether ether ketone)
PES = poly(ether sulfone)
S-PEEK = sulfonated poly(ether ether ketone)

Greek Letters

δ = thickness of the boundary layer (m)
τ = transition time (s)

References and Notes

(1) Ibanez, R.; Stamatialis, D. F.; Wessling, M. *J. Membr. Sci.* **2004**, *239*, 119.
(2) Spiegler, K. S. *Desalination* **1971**, *9*, 367.
(3) Rosberg, N. W.; Tirell, C. E. *Ind. Eng. Chem. Res*. **1957**, *49*, 780.
(4) Indusekhar, V. K.; Meares, P. In *Physicochemical Hydrodynamics II*; Spalding, D. B., Ed.; Advance Publications: London, 1977, p 1031.
(5) Forgacs, C.; Ishibashi, N.; Leibovitz, J. *Desalination* **1972**, *10*, 181.
(6) Simons, R. *Desalination* **1979**, *28*, 41.
(7) Krol, J. J.; Wessling, M.; Strathmann, H. *J. Membr. Sci.* **1999**, *162*, 145.
(8) Krol, J. J.; Wessling, M.; Strathmann, H. *J. Membr. Sci.* **1999**, *162*, 155.
(9) Zabolotsky, V. I.; Nikonenko, V. V.; Pismenskaya, N. D.; Laktionov, E. V.; Urtenov, M. K.; Strathmann, H.; Wessling, M.; Koops, G. H. *Sep. Purif. Technol.* **1998**, *14*, 255.
(10) Zabolotsky, V. I.; Pismenskaya, N. D.; Nikonenko, V. V. *Elektrokhimiya* **1998**, *26*, 707.
(11) Choi, J.-H.; Lee, H.-J.; Moon, S.-H. *J. Colloid Interface Sci.* **2001**, *238*, 188.
(12) Tanaka, Y. *J. Membr. Sci.* **2002**, *203*, 227.
(13) Belova, E. I.; Lopatkova, G. Y.; Pismenskaya, N. D.; Nikonenko, V. V.; Larchet, C.; Pourcelly, G. *J. Phys. Chem. B* **2006**, *110*, 13458.
(14) Simons, R. *Electrochim. Acta* **1985**, *30*, 275.
(15) Simons R. *Nature* **1979**, *280*, 824.
(16) Rubinstein, I.; Warshawsky, A.; Schechtman, L.; Kedem, O. *Desalination* **1984**, *51*, 55.
(17) Block, M.; Kitchener, J. A. *J. Electrochem. Soc.* **1966**, *113*, 947.
(18) Reich, S.; Gavish, B.; Lifson, S. *Desalination* **1977**, *24*, 295.
(19) Li, Q.; Fang, Y.; Green, M. E. *J. Colloid Interface Sci*. **1983**, *91*, 412.
(20) Zabolotsky, V. I.; Nikonenko, V. V.; Pismenskaya, N. D. *J. Membr. Sci.* **1996**, *119*, 171.
(21) Rubinstein, I.; Maletzki, F. *J. Chem. Soc., Faraday Trans.* **1991**, *87*, 2079.
(22) Maletzki, F.; Rosler, H.-W.; Staude, E. *J. Membr. Sci*. **1992**, *71*, 105.
(23) Dukhin, S. S.; Mishchuk, N. A. *J. Membr. Sci*. **1993**, *79*, 199.
(24) Rubinstein, I; Zaltzman, B.; Kedem, O. *J. Membr. Sci*. **1997**, *125*, 17.
(25) Rubinstein, I.; Zaltzman, B. *Phys. Rev. E* **2000**, *62*, 2238.
(26) Rubinstein, I.; Zaltzman, B.; Pretz, J.; Linder, C. *Russ. J. Electrochem*. **2002**, *38*, 956.
(27) Rubinstein, I.; Zaltzman, B.; Pundik, T. *Phys. Rev. E* **2002**, *65*, 041507.
(28) Rubinstein, I.; Zaltzman, B. *Math. Models Methods Appl. Sci*. **2001**, *11*, 263.
(29) Rubinstein, I.; Zaltzman, B. *Phys. Rev. E* **2003**, *68*, 032501.
(30) Rubinstein, I.; Zaltzman, B.; Lerman, I. *Phys. Rev. E* **2005**, *72*, 011505.
(31) Alexandrov, R. S.; Grigin, A. P.; Davydov, A. P. *Russ. J. Electrochem*. **2002**, *38*, 1216.
(32) Baygents, J. C.; Baldessari, F. *Phys. Fluids* **1998**, *10*, 301.
(33) Bruinsma, R.; Alexander, S. *J. Chem. Phys*. **1990**, *92*, 3074.
(34) Buchanan, M. E.; Saville, D. A. In *Proceedings of the AIChE Annual Meeting*; American Institute of Chemical Engineers (AIChE): New York, 1999.
(35) Grigin, A. P. *Sov. Electrochem*. **1985**, *21*, 48.
(36) Grigin, A. P. *Sov. Electrochem*. **1992**, *28*, 247.
(37) Lerman, I.; Rubinstein, I.; Zaltzman, B. *Phys. Rev. E* **2005**, *71*, 011506.
(38) Rubinstein, I.; Zaltzman, T.; Zaltzman, B. *Phys. Fluids* **1995**, *7*, 1467.
(39) Dukhin, S. S. *Adv. Colloid Interface Sci.* **1991**, *35*, 173.
(40) Zholkovskij, E. K.; Vorotyntsev, M. A.; Staude, E. *J. Colloid Interface Sci*. **1996**, *181*, 28.
(41) Dukhin, S. S.; Derjaguin, B. V. *Electrophoresis*, 2nd ed.; Nauka: Moscow, U.S.S.R., 1976.
(42) Bazant, M. Z.; Squires, T. M. *J. Fluid Mech*. **2004**, *509*, 217.
(43) Bazant, M. Z.; Squires, T. M. *Phys. Rev. Lett.* **2004**, *92*, 066101.
(44) Bazant, M. Z.; Thornton, K.; Ajdari, A. *Phys. Rev. E* **2004**, *70*, 021506.
(45) Ben, Y.; Chang, H. C. *J. Fluid Mech.* **2002**, *461*, 229.
(46) Dukhin, S. S.; Mishchuk, N. A. *Colloid J. USSR* **1989**, *51*, 570.
(47) Dukhin, S. S.; Mishchuk, N. A.; Takhistov, P. B. *Colloid J. USSR* **1989**, *51*, 616.
(48) Mishchuk, N.; Gonzalez-Caballero F.; Takhistov, P. *Colloids Surf. A: Physicochem. Eng. Aspects* **2001**, *181*, 131.
(49) Balster, J.; Krupenko, O.; Pünt, I.; Stamatialis, D. F.; Wessling, M. *J. Membr. Sci*. **2005**, *263*, 137.
(50) Wilhelm, F. G.; Punt, I. G. M.; van der Vegt, N. F. A.; Strathmann, H.; Wessling, M. *J. Membr. Sci.* **2002**, *199*, 167.
(51) Mulder, M. *Basic Principles of Membrane Technology*, 2nd ed.; Kluwer Academic Publishers: Dordrecht, The Netherlands, 1996; Chapter 3.
(52) Bard, A. J. *Electrochemical Methods: Fundamentals and Applications*; John Wiley & Sons: New York, 1980.
(53) Delahay, P. Chronoamperometry and chronopotentiometry. In *Treatise on Analytical Chemistry*; Kolthoff, I. M., Elving, P. J., Eds.; John Wiley & Sons: New York, 1963; Part 1, Vol. 4, pp 2233−2265.
(54) Sawyer, D. T. *Experimental Electrochemistry for Chemists*; John Wiley & Sons: New York, 1974.
(55) Choi, J.-H; Moon, S.-H. *J. Membr. Sci*. **2001**, *191*, 225.
(56) Choi, J.-H.; Kim, S.-H.; Moon, S.-H. *J. Colloid Interface Sci.* **2001**, *241*, 120.
(57) Rubinstein, I.; Staude, E.; Kedem, O. *Desalination* **1988**, *69*, 101.
(58) Taky, M.; Pourcelly, G.; Lebon, F.; Gavach, C. *J. Electroanal. Chem.* **1992**, *336*, 171.
(59) Rosler, H.-W.; Maletzki, F.; Staude, E. *J. Membr. Sci.* **1992**, *72*, 171.
(60) Robinson, R. A.; Stokes, R. H. *Electrolyte Solutions*, 2nd ed.; Butterworths: London, 1959.
(61) Volodina, E.; Pismenskaya, N.; Nikonenko, V.; Larchet, C.; Pourcelly, G. *J. Colloid Interface Sci.* **2005**, *285*, 247.